Nuclear Engineering and Technology 52 (2020) 1792–1797

Contents lists available at ScienceDirect

Nuclear Engineering and Technology

journal homepage: www.elsevier.com/locate/net

Original Article

X-ray and gamma ray shielding behavior of concrete blocks

Christian Geovanni Hernandez-Murillo [a, *], J. Rafael Molina Contreras [a], Luis Alberto Escalera-Velasco [a], Héctor Asael de Leon-Martínez [a], José Antonio Rodriguez-Rodriguez [b], Héctor Rene Vega-Carrillo [b]

[a] Instituto Tecnológico de Aguascalientes, Av. Adolfo López Mateos 1801 Ote. Fracc. Bona Gens, 20256 Aguascalientes, Ags, Mexico
[b] Unidades Académicas Ingeniería II y Estudios Nucleares de la, Universidad Autónoma de ZacatecasC, Ciprés 10, Fracc. La Peñuela, 98068, Zacatecas, Zac, Mexico

ARTICLE INFO

Article history:
Received 1 August 2019
Received in revised form
16 December 2019
Accepted 8 January 2020
Available online 10 January 2020

Keywords:
Concrete block
X rays
Gamma-rays
XCOM
Shielding

ABSTRACT

The shielding characteristics of two concrete blocks, widely used in the building industry in Mexico have been determined. These characteristics include the mass interaction coefficients, the linear attenuation coefficients and the half-value layers. The energy-dispersed X-ray fluorescence shows that the percentage mass content of each atom in the sample, and the atomic volume of the constituent elements of a material, plays an important role in its shielding capabilities. The total linear attenuation coefficients and the half-value layers were analyzed for a set of photon energies related to X-rays for diagnosis and cancer treatment with linear accelerators. Our results show that the concrete blocks have similar photon attenuation coefficients than the Portland concrete and better features than gypsum.

1. Introduction

Transitions between nuclear energy states result in photons of X-rays and gamma rays, which are also the most energetic of the electromagnetic spectrum. That is, ionizing photons. The most important interaction mechanisms of these photons with matter are summarized in three. 1. The photoelectric effect, where an electron that absorbs an incident photon, acquires enough energy to detach itself from its atom. This mechanism dominates in low energies, and in it, a photon of the order of keV, in its interaction with matter, is absorbed by the atoms of the material, and its energy, passes mostly to the deeper layers of the atom; resulting in the expulsion of electrons. The expulsion of electrons leaves a hole in the electronic configuration of the atom; so, the atom is rearranged to fill the gap with the available electrons, and in the process, X-rays are generated. These X-rays are characteristic of each atom. The probability that this mechanism will happen is directly related to the atomic number Z of the constituent elements of the atom involved in the process. 2. The Compton effect, where the incident photon is deflected a certain angle from its original path by an electron in the sample. This mechanism dominates the intermediate energies and the result is that, in the process, the photon only transfers part of its energy to the electron. So, anyway, the deviated photons are very energetic. The probability of this effect increases linearly with the atomic number Z of the atom. And 3, the creation of pairs, where an incident photon with an energy of at least 1.02 MeV, when crossing a material medium, can cause the production of pairs of particles (electron, positron) when absorbed in the proximity of a Coulombian nuclear field. It dominates in the high energies in its interaction with matter and the probability that it happens, depends again on the atomic number Z of the atoms and the energy of the photon.

The attenuation coefficients on the other hand, express in macroscopic units the microscopic effective sections of all elementary processes of the interaction of ionizing radiation with matter. The fundamental processes in the interactions of photons with matter may be dominant or more likely. The fundamental processes are dominant when they cause the photon to lose more energy. In water, the photoelectric effect dominates below 50 keV. Between 50 and 100 keV, the photoelectric effect and the Compton effect are important, between 200 keV and 2 MeV, dominates the Compton effect, between 5 and 10 MeV the Compton effect remains

* Corresponding author. Instituto Tecnológico de Aguascalientes, Av. Adolfo López Mateos 1801 Ote. Fracc. Bona Gens, 20256, Aguascalientes, Ags, Mexico.
E-mail address: tecelectrigeo@live.com.mx (C.G. Hernandez-Murillo).

https://doi.org/10.1016/j.net.2020.01.007

dominant, but the pair production begins to appear, and from 50 to 100 MeV the production of pairs is dominant. In general, the photoelectric effect dominates in low energies, the Compton effect in intermediate energies and the production of pairs in high energies. In addition, the region of predominance of the Compton effect narrows with increasing Z. This means that the relative importance of the photoelectric effects, Compton and the production of pairs, will depend both on the energy of the photon, and on the availability of electrons in the material and therefore, of the atomic number Z.

The Energy Dispersed X-Ray Fluorescence (EDXRF), is a non-destructive technique used to determine in this work the chemical composition of our samples. In EDXRF, the sample is excited with X-rays that provide enough energy to the electrons of the innermost bands of the constituent atoms of the materials, as to separate them from their atoms. The released electrons leave a vacancy that immediately tends to be filled by the electrons of the outermost layers to preserve the initial state of energy. In the process, the atoms of the material, emit fluorescent X-rays characteristic of the constituent atoms of the irradiated sample. The constituent elements and even the percentages of mass that each atom contributes to the sample can be determined by measuring the emitted radiation. Measurements of the X-ray transmission, can give information regarding the shielding capacity of a material.

Currently there are several fields where the ionizing radiation is used. Its increase in medical, agricultural, scientific research, and technological fields among others, motivates to evaluate the interaction between the ionizing radiation and building materials. Improper use of the ionizing radiation is a risk for human health [1], so, the management of the radiation sources must be done following safety protocols [2]. This means, that the design of shields and the evaluation of enclosures that house ionizing sources is a key factor in radiological safety.

In the literature, have been reported several studies of natural and artificial materials, used to shield X-ray, gamma-rays, and neutrons. Artificial materials include: gypsum [3], concrete [4–7], concrete with aggregates [8–12], glass [13], poly vinyl alcohol [14], ethylene propylene diene terpolymer [15], lead, barium and sodium oxides [16], epoxy resin matrix filled with PbO [17], carbon steel and stainless steel [18]. The photon attenuation characteristics are also investigated for semiconductors [19] in the aim to design novel radiation detectors. Among natural materials are: the Mexican onyx [20], wood [21], and quarry stone [22] among others. In all the cases, the shielding features (mass attenuation coefficients (μ_m); half value-layer ($t_{1/2}$) and the linear attenuation coefficients (μ), among others) were determined using experimental methods and/or calculations using the XCOM code [23], the WinXCOM [24] code or Monte Carlo codes like MCNP5 [25] and GEANT [26].

The experimental methods normally used to validate the calculated and actual linear attenuation coefficients, are often photon transmission experiments which can use a narrow or a broad beam geometry.

Recent studies show that gypsum and woods, are widely used in the construction industry due to their availability and relative low costs. Gypsum on the other hand, although, its low-Z and density, is widely used in medical facilities, particularly for those that house X-ray machines for diagnostics. Due to this, its shielding features are well known [27].

Worldwide, concrete is used extensively in the construction industry, but traditional knowledge, experience and available natural resources have allowed other materials to be used. To get the most out of these materials, it is necessary to characterize them; particularly in its ability to shield ionizing photons. In Mexico, the National Institute of Statistics and Geography (INEGI), reports that 88.7% of the walls built in Mexico are made with durable materials as: concrete blocks, quarry tuffs, bricks, concrete and stone [28]. Some of the built facilities house X-rays devices or gamma-ray sources. These facilities include hospitals, industrial facilities, and installations for research and for education. However, although construction materials are well identified in Mexico, there are no shielding characteristics, in some cases, even of those materials commonly used for constructions as the concrete blocks. The lack of this information makes very difficult the shielding design, and the evaluation of facilities made with these materials.

The objective of this work was to study the shielding characteristics of two concrete structures widely use in the construction industry in Mexico: solid and hollow blocks.

2. Materials and methods

The materials used in this research, were parallelepipeds manufactured industrially by PRELOSA company with a 1: 5: 2 volumetric ratio of Portland cement, sand and crushed gravel [29]. All the blocks used in this experiment were obtained in the local market in the city of Aguascalientes, Mexico and were concrete blocks certified in accordance with the current Mexican regulations, which establish a durability of more than 100 years for the blocks, a compressive force of 150 kg/cm^2 for the solid block and 90 kg/cm^2 for the hollow one; and a compressive strength in low walls of 317 kg/cm^2 for the solid block and 259 kg/cm^2 for the hollow one.

The two types of concrete blocks used in this work, were hollow parallelepipeds with measures of 39x19 × 19 cm, and five walls 3 cm thick, labeled as (LB_AGS); and solid concrete blocks with measures of 28x14 × 9 cm labeled as (B_AGS). See Fig. 1a) and b).

2.1. Determination of the elemental composition

To determine the elemental composition, ten pieces of approximately 15 g of each block were taken, crushed, passed through 1 mm mesh and mixed. Then, approximately 20 g of the mixtures were characterized by EDXRF using a Bruker spectrometer model S2 PUMA, with a silver-white X-ray tube (Ag) and an XFlash detector.

2.2. Determination of the density

The densities of both B_AGS and LB_AGS concrete blocks were measured following the NMX-C-164OnNCCE-2014 Mexican Standard [30]. Samples of 60.494 ± 0.001 g of the B_AGS block, and 67.015 ± 0.001 g of the LB_AGS block, were grinded. The obtained powder was passed through a 1 mm mesh and were heated to 100 °C for 24 h in a FELISA oven model FE-291AD of 1100 W. The powder was removed and weighted three times in order to determine the humidity lost. According to the standard, 50 g of each sample with 150 ± 1 ml of deionized water was poured into a test tube of 250 ± 1 ml and then the volume of water displaced by the concrete samples was measure. The density was calculated with the volume displaced by the water and the weight of the samples.

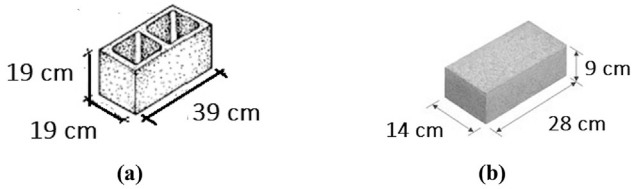

Fig. 1. (a) Solid concrete block. (b) Hollow concrete block.

2.3. Determination of the mass interaction coefficients

To know how strongly our B_AGS and LB_AGS blocks, absorb light at a given wavelength per unit mass, we calculated their mass interaction coefficients μ_m (E) considering the three most important interaction mechanisms of photons with matter.

The calculations were done with the XCOM code for photons between 1 keV and 100 GeV including a set of energies widely used for mammography, dental machines, bone radiographies and cancer treatment in the medical field. In these calculations, the mass percentages of each constituent element of the concrete blocks were the key factor. With the mass interaction coefficients and density, were obtained the total linear attenuation coefficients of our samples. And with the total linear attenuation coefficients, were determined the half-value layer (HVL) for both B_AGS and LB_AGS blocks for the selected group of photon energies mentioned before. For comparison, the same calculations were carried out for natural Gypsum and Portland concrete.

Calculations were validated using a 0.662 MeV γ-rays source in a transmission experiment as the one shown in Fig. 2.

3. Results and discussion

3.1. Elemental composition and density

In this discussion were taken into account just the constituent elements of the materials that contribute with more than two percent to the total mass of the mentioned samples. The elements that have been considered for the analysis, add up to 94.39% of the total mass of the Portland concrete and 99.37% for the B_AGS and 99.23% for the LB_AGS blocks respectively.

As can be noticed in Table 1, the element with the highest mass percentage is O in all the samples. In the case of the B_AGS and LB_AGS blocks, this can be attributed to the formation of oxides with all the elements shown in the Table. The second element with a large percentage in both concrete blocks is Si and it is higher in the Portland concrete. The approximately 22% of Si contained in both B_AGS and LB_AGS concrete blocks is probably due to the amount of sand used during their manufacture. In Portland concrete on the contrary, it's almost thirty-four percent of Si, instead it may be due to the formulation used. Gypsum on the other hand, does not contain Si.

It is also interesting that the two B_AGS, and LB_AGS concrete blocks, have Mg, K and Fe in addition to the four elements O, Al, Si and Ca that they share with Portland concrete. In addition to this, it is striking that the concrete blocks B_AGS, and LB_AGS contain almost five times more Ca and little more Al than the Portland concrete. The densities measured for the B_AGS, and LB_AGS concrete blocks are also shown in Table 1 and how it looks, their densities are slightly greater than the density of the Portland concrete, what is reasonable to attribute to the presence of Mg, K and Fe and the extra amount of mass due to Ca and Al. By adding to this analysis, the atomic masses of the constituent elements in each sample, is possible to have the image of how each constituent element contributes to the densities of the samples. The atomic masses of K and Fe are among the largest of the constituent elements of concrete blocks, and they are not contained in the Portland concrete, at least in a percentage of two percent, so contribute to the densities of the B_AGS, and LB_AGS blocks, but not to the density of the Portland concrete. And if it is also added that the total analyzed masses of the concrete blocks are greater than that of the Portland concrete, it is understood that the densities of the concrete blocks are greater than that of the Portland concrete as it does at least with the number of elements taken for the analysis. So, the slightly large density of our concrete blocks is mainly due to the presence of Fe, and Mg in their elemental composition, just because their densities [31]. The density of the gypsum is explained by a similar reasoning considering that it contains only three elements.

Fig. 2. Experimental set up.

3.2. Mass and linear interaction coefficients

Fig. 3 shows the mass interaction coefficients of the LB_AGS concrete block. For this kind of concrete block as it can be seen, the probability of occurrence of the photoelectric effect is higher and goes from 1 keV to 60 keV. The Compton effect begins to dominate from 60 keV, until it intersects with the probability of occurrence of the nuclear pair production, which starts around 15 MeV, then the nuclear pair production dominates until 100 GeV. What stands out from these results is the narrow predominance of the photoelectric and the Compton effects compared to the region in which the nuclear pair production predominates.

The mass interaction coefficients, seen from the microscopic perspective, as stated in the introduction, are related to the effective area that a compound interposes to the impact of the photon. Therefore, they give an account of the force with which such compound absorb light at a given frequency per unit mass. Having nothing to do with density, they are constricted to the amount of mass of the material and the type of elements that constitute the material, and the percentage of mass with which each element contributes to the total mass. This is what the results obtained with the XCOM code show in Fig. 3 for the sum of the set of the seventeen constituent elements of the LB_AGS concrete block.

The results obtained with the XCOM code, as can be seen in Fig. 3, nevertheless mask the individual effects not only of the atomic volume of each element, which of course has to do with the effective section, but of the amount of mass that each element contributes to the total mass. This reasoning is valid by assuming for example that a lead percentage of 0.000056 of the total mass of the mixture in the analyzed block (not shown in Table 1), does not contribute equal than 42.57% of oxygen (also of the total mass of the mixture) to the attenuation. A type of approach like this is not mentioned in the literature, but as we see it, such knowledge would have a predictive character in the search for new materials, particularly when aggregates are mixed with materials that are already well characterized. So, in order to determine how the constituent elements, contribute to the attenuation capacity of the material, in this work it was considered that the probability of occurrence of the aforementioned dominant effects is increased in terms of the atomic volume of the constituent elements of the material and the mass available for the impact. Theory says that the mass attenuation coefficients μ/ρ are highly dependent on the cross

Table 1
Constitutive Elements that Contribute more than Two Percent to the Total Mass.

Atomic Number	Element	B_AGS (% mass)	LB_AGS (% mass)	GYPSUM (% mass)	P. Concrete (% mass)
8	O	42.39	42.57	47.01	52.91
12	Mg	3.95	3.46	–	–
13	Al	4.14	4.3	–	3.38
14	Si	22.22	21.79	–	33.7
16	S	–	–	23.55	–
19	K	2.12	2	–	–
20	Ca	21.83	21.78	29.44	4.4
26	Fe	2.42	2.69	–	–
	Density	**2.32 ± 0.03(g/cm^3)**	**2.32 ± 0.03(g/cm^3)**	**0.73(g/cm^3)**	**2.3(g/cm^3)**

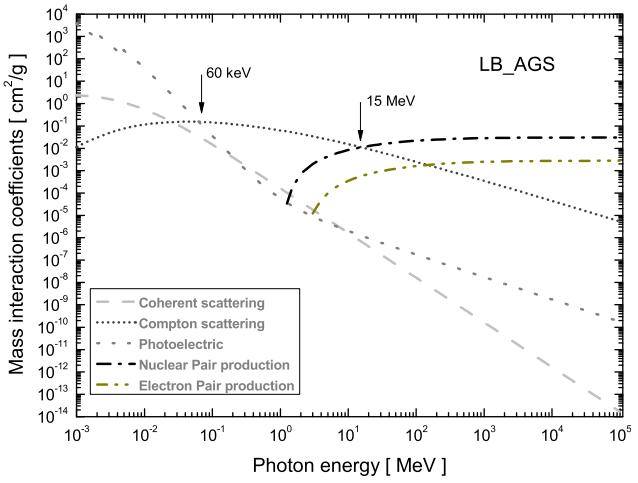

Fig. 3. Mass interaction coefficients of LB-AGS block.

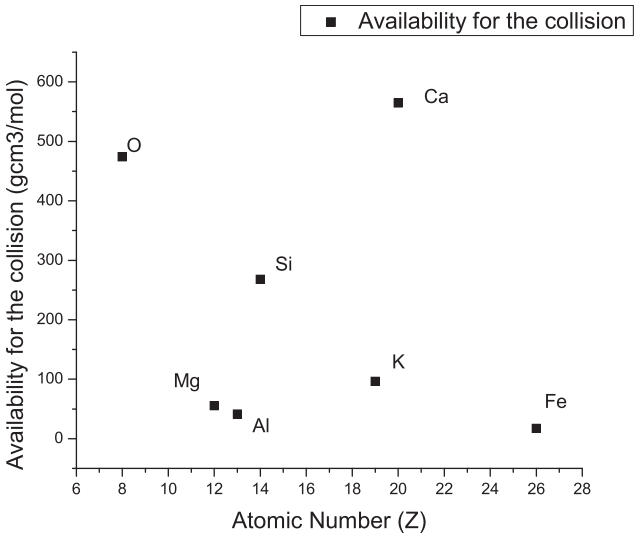

Fig. 4. Availability for the collision.

section per atom as,

$$\mu \Big/ \rho = \sigma_{tot}/\mu A \tag{1}$$

Where σ_{tot} is the total cross section available for an interaction with the photon, A is the is the relative atomic mass of the element of interest and μ is the atomic mass unit related to the nuclide ^{12}C.

With this theoretical basis, in this work, we have defined the availability for the collision per atom and mass that each element contributes to the total mass of the material, as the multiplication of the volume by the percentage of mass contributed by each element to the total mass of the material. For analysis issues, we have considered only the seven elements of the LB_AGS concrete block that contribute more than two percent of its total mass. Together, however, these seven elements make more than ninety-nine-point twenty-three percent of the total mass. Fig. 4 shows the availability for the collision of the seven elements of the LB_AGS concrete block. As can be seen, the result is overwhelming. Shows with a clear clarity that the highest availability for the collision, corresponds to Ca and then O, and yet, they are not the elements with the highest atomic number; which in a sense is surprising, since it is believed that the greater the atomic number, the greater the capacity for shielding. With these results, it is reasonable to think that Ca and O are the elements that contribute most to the attenuation capacity of the LB_AGS concrete block. Then, from highest to lowest, the contribution to the attenuation of the five remaining elements is due to Si, K, Mg Al and Fe. What attracts most the attention in these results is that, the Fe, being the element with the highest atomic number, and also the one with the highest atomic mass of the seven elements, it is in fact, the one that offers the small availability for the collision to the incident photon, and by the same logic, the one that contributes the least in the process of attenuation of the LB_AGS concrete block. This can be attributed to both, the low percentages of mass with which Fe contribute to the total mass of the LB_AGS concrete block and to its so small volume.

The methodology used in this work using EDXRF and the XCOM code has proven to be a powerful tool to unravel what was barely felt in the study of the interaction between ionizing radiation and matter.

The performance shown in Fig. 3, and the calculations of the total linear attenuation coefficients, allows to say that the photoelectric effect is the main interaction process for photons with E < 80 keV. In the Photoelectric effect, as it is well known, the incident photon is fully absorbed, which causes the expulsion of some electrons, mainly from the K-shell. Fig. 3 shows this behavior in the line shape of the photoelectric effect for energies below 10 KeV, where the probability of occurrence of the photoelectric effect, does not follow a smooth line, but a jagged line with jumps in specific regions of the spectrum. These changes in the line shape, correspond exactly to the energies of the electrons expelled from the K layers of the Si (1.84 keV), Mg (1.31 keV), Al (1.56 keV), K (3.61 keV), Ca (4.04 keV), and Fe (7.11 keV) atoms. These expelled electrons are quickly stopped in the material due to Coulombian interactions, becoming X-rays of the Bremsstrahlung type. These X-rays are also the ones that are most likely to be absorbed for E < 80 keV. This means that the LB_AGS concrete block can be used to shield X-ray equipment for mammography and dental images, which are manufactured with 30, 60, 70, and 80 kV X-ray tubes.

For practical purposes and comparison, the linear attenuation

coefficients, calculated with the density of the samples and the mass interaction coefficients, were used to determine the half-value layer needed to attenuate to 50% the incident photons. Fig. 5 shows the half-value layer of Portland Concrete and the LB_AGS concrete block. What comes out in this figure is that a smaller thickness of the LB_AGS concrete is required to attenuate the photon energies in specific regions of the electromagnetic spectrum. Although the differences are minimal, they can be distinguished in particular from 6 to 18 MeV. This can definitely be attributed to the mass that the elements used for the analysis make to the total mass. The analyzed masses were, 94.39 for Portland concrete, and 99.27 for the LB_AGS block.

Here, we have demonstrated that the photon attenuation features of the Portland concrete and the LB_AGS concrete block depend on the percentage of mass that each atom contributes to the total mass of the material. This confirms that the concrete block reported in this work, have a great performance for the energies related with image diagnostic and cancer treatment.

The data calculated with XCOM were validated in this work for 0.662 MeV using a point-like ^{137}Cs source. The degree of confidence between the experimental data and the functions adjusted to the attenuation law, was greater than ninety-five percent.

4. Conclusions

It is shown that concrete blocks can be used in the shield design for ionizing photons below 80 keV. Making suitable to design primary and secondary barriers for facilities hosting X-rays for dental diagnosis.

We have shown that the amount of mass and the atomic volume of the constituent elements of a material determine its ability to shield.

Availability for collision is defined and used for the first time in this work.

It is shown that the availability for the collision is an effective parameter to determine how much the constituent elements of the materials contribute to the attenuation.

This work reports for the very first time the radiation shielding characteristics of two concrete blocks widely used for constructions in Mexico. Results reported, could be useful to carry on experiments in order to verify some of the shielding features of these materials.

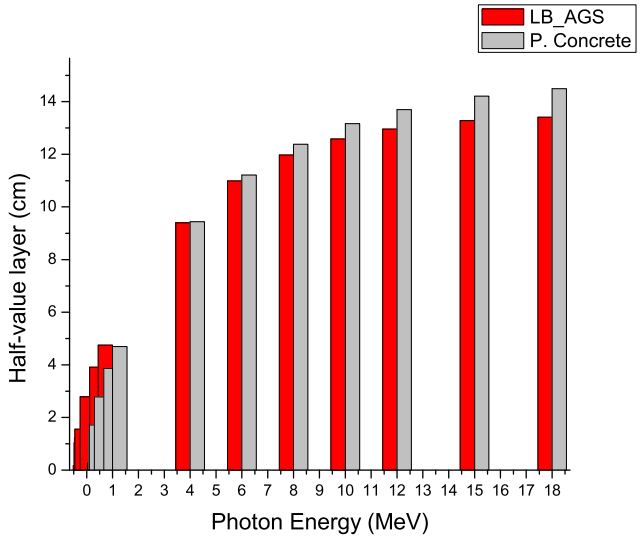

Fig. 5. Half-value layer of Portland concrete and LB_AGS concrete block in terms of the wavelength.

Declaration of competing interest

The authors declare that they have no known competing financial interests or personal relationships that could have appeared to influence the work reported in this paper.

Acknowledgements

The first, third and fourth authors thanks to CONACYT for the scholarship granted to pursue the postgraduate studies.

Appendix A. Supplementary data

Supplementary data to this article can be found online at https://doi.org/10.1016/j.net.2020.01.007.

References

[1] Q.C. Meisinger, C.M. Stahl, M.P. Andre, T.B. Kinney, I.G. Newton, Radiation protection for the fluoroscopy operator and staff, Am. J. Roentgenol. 207 (2016) 745–754.
[2] NCRP, Management of exposure to ionizing radiation: radiation protection guidance for the United States report No. 180, J. Radiol. Prot. 39 (2018) 4–9.
[3] K.S. Mann, J. Singla, V. Kumar, G.S. Sidhu, Verification of some building materials as gamma-ray shields, Radiat. Prot. Dosim. 151 (2012) 183–195.
[4] T. Croymans, F. Leonardi, R. Trevisi, C. Nuccetelli, S. Schreurs, W. Schroeyers, Gamma exposure from building materials – a dose model with expanded gamma lines from naturally occurring radionuclides applicable in non-standard rooms, Constr. Build. Mater. 159 (2018) 768–778.
[5] S.S. Obaid, D.K. Gaikwad, P.P. Pawar, Determination of gamma ray shielding parameters of rocks and concrete, Radiat. Phys. Chem. 144 (2018) 356–360.
[6] S. Özen, C. Sengül, T. Erenoğlu, Ü. Çolak, Properties of Heavyweight concrete for structural and radiation shielding purposes, Arabian J. Sci. Eng. 41 (2016) 1573–1584.
[7] I. Akkurt, H. Akyıldırım, B. Mavi, S. Kilincarslan, C. Basyigit, Photon attenuation coefficients of concrete includes barite in different rate, Ann. Nucl. Energy 37 (2010) 910–914.
[8] H. Baltas, M. Sirin, A. Celik, İ. Ustabas, A.M. El-Khayatt, Radiation shielding properties of mortars with minerals and ores additives, Cement Concr. Compos. 97 (2019) 268–278.
[9] M.I. Sayyed, H.O. Tekin, O. Kilicoglu, O. Agar, M.H.M. Zaid, Shielding features of concrete types containing sepiolite mineral: comprehensive study on experimental, XCOM and MCNPX results, Results in Physics 11 (2018) 40–45.
[10] M. Alwaeli, Investigation of gamma radiation shielding and compressive strength properties of concrete containing scale and granulated lead-zinc slag wastes, J. Clean. Prod. 166 (2017) 157–162.
[11] M. Çullu, H. Ertaş, Determination of the effect of lead mine waste aggregate on some concrete properties and radiation shielding, Constr. Build. Mater. 125 (2016) 625–631.
[12] E. Gallego, A. Lorente, H.R. Vega-Carrillo, Testing of a high-density concrete as neutron shielding material, Nucl. Technol. 168 (2009) 399–404.
[13] M.G. Dong, O. Agar, H.O. Tekin, O. Kilicoglu, K.M. Kaky, M.I. Sayyed, A comparative study on gamma photon shielding features of various germanate glass systems, Compos. B Eng. 165 (2019) 636–647.
[14] S.A. Issa, A.M.A. Mostafa, T.A. Hanafy, M. Dong, X. Xue, Comparison study of photon attenuation characteristics of Poly vinyl alcohol (PVA) doped with Pb $(NO_3)2$ by MCNP5 code, XCOM and experimental results, Prog. Nucl. Energy 111 (2019) 15–23.
[15] T. Özdemir, A. Güngör, I.K. Akbay, H. Uzun, Y. Babucçuoglu, Nano lead oxide and EPDM composite for development of polymer-based radiation shielding material: gamma irradiation and attenuation tests, Radiat. Phys. Chem. 144 (2018) 248–255.
[16] A. Kumar, R. Kaur, M.I. Sayyed, M. Rashad, M. Singh, A.M. Ali, Physical, structural, optical and gamma ray shielding behavior of (20+x) PbO – 10 BaO – 10 Na_2O – 10 MgO – (50-x) B_2O_3 glasses, Phys. B Condens. Matter 552 (2019) 110–118.
[17] M. Dong, X. Xue, S. Liu, H. Yang, Z. Li, M.I. Sayyed, O. Agar, Using iron concentrate in Liaoning Province, China, to prepare material for X-Ray shielding, J. Clean. Prod. 210 (2019) 653–659.
[18] V.P. Singh, N. Badiger, Study of mass attenuation coefficients, effective atomic numbers and electron densities of carbon steel and stainless steels, Radioprotection 48 (2013) 431–443.
[19] M.C. Veale, L.L. Jones, B. Thomas, P. Seller, M.D. Wilson, K. Iniewski, Improved spectroscopic performance in compound semiconductor detectors for high rate X-ray and gamma-ray imaging applications: a novel depth of interaction correction technique, Nucl. Instrum. Methods Phys. Res. 927 (2019) 37–45.
[20] C.A. Márquez-Mata, H.R. Vega-Carrillo, J.M. Chávez Mata, J.J. Araiza-Ibarra, J.J. Ortega-Sigala, M.I. Escalona-Llaguno, Á. García-Duran, Characterization of six types of Mexican Onyx, Appl. Radiat. Isot. 146 (2019) 139–144.

[21] S. Yasmin, M.U. Khandaker, B. S Barua, M.N. Mustafa, F.U.Z. Chowdhury, M.A. Rashid, D.A. Bradley, Ionizing Radiation Shielding Effectiveness of Decorative Building Materials (Porcelain and Ceramic Tiles) Used in Bangladeshi Dwellings, Indoor and Built Environment, 2018, https://doi.org/10.1177/1420326X18798883.
[22] H.R. Vega-Carrillo, K.A. Guzman-Garcia, A. Rodriguez-Rodriguez, C.A. Juarez-Alvarado, V.P. Singh, H.A. de Leon-Martinez, Photon and neutron shielding features of quarry tuff, Ann. Nucl. Energy 112 (2018) 411–417.
[23] M.J. Berger, J.H. Hubbell, S.M. Seltzer, J. Chang, J.S. Coursey, R. Sukumar, D.S. Zucker, K. Olsen, XCOM: Photon Cross Sections Database, National Institute of Standards and Technology, Gaithersburg, MD, 2010 [Online] Available:, version 1.5. http://physics.nist.gov/xcom. (Accessed 26 May 2019).
[24] L. Gerward, N. Guilbert, K. Bjorn Jensen, H. Levring, X-ray absorption in matter: re-engineering XCOM, Radiat. Phys. Chem. 60 (2001) 23–24.
[25] X-5 Monte Carlo Team, MCNP – a general Monte Carlo N-particle transport code, in: Volume I: Overview and Theory, Los Alamos Natl. Lab., 2003. LA-UR-03-1987, Version 5.
[26] S. Agostinelli, J. Allison, K. Amako, Geant4 - a simulation toolkit, Nucl. Instrum. Methods A 506 (2003) 250–303.
[27] NCRP, Structural Shielding Design for Medical X-Ray Imaging Facilities, National Council of Radiation and Measurements, 2005. Report No. 172.
[28] INEGI, Percentage of Housing with Walls of Solid Materials, National Institute of Statistics and Geography of Mexico, 2019. http://en.www.inegi.org.mx/.
[29] J. Arrieta Freyre, E. Peña Herrera Deza, Fabricación y bloques de concreto con una mesa vibradora. Centro Peruano Japonés de Investigaciones Sísmicas y Mitigación de Desastres, Programa Científico, 2001, pp. 10–15. PC-CISMID, 1999-2000.
[30] NMX, Building Industry-Aggregates-Determination of the Specific Mass and Water Absorption of Coarse Aggregates, Mexican Standard, 2014. NMX-C-164-ONNCCE-2014.
[31] Lenntech Data, Elementos químicos ordenados por su masa atómica [Online] Available: https://www.lenntech.es/tabla-peiodica/masa-atomica.htm, 2019.